# Bistability suppression and low threshold switching using frozen light at a degenerate band edge waveguide

**Nadav Gutman,**[1,*] **Andrey A. Sukhorukov,**[2] **Falk Eilenberger,**[3] **and C. Martijn de Sterke**[1]

[1]*IPOS and CUDOS, School of Physics, University of Sydney, NSW 2006, Australia*
[2]*Nonlinear Physics Centre, Research School of Physics and Engineering, Australian National University, Canberra ACT 0200, Australia*
[3]*Institute of Applied Physics, Abbe Center of Photonics, Friedrich-Schiller-Universität Jena, Max-Wien-Platz 1,07743 Jena, Germany*
[*]*nadav@physics.usyd.edu.au*

**Abstract:** We predict that nonlinear waveguides which support frozen light associated with a degenerate photonic band edge, where the dispersion relation is locally quartic, exhibit a tunable, all-optical switching response. The thresholds for switching are orders-of-magnitude lower than at regular band edges. By adjusting the input condition, bistability can be eliminated, preventing switching hysteresis.



**OCIS codes:** (190.1450) Bistability; (250.4390) Nonlinear optics, integrated optics.

## References and links

1. H. M. Gibbs, *Optical Bistability: Controlling Light with Light* (Academic Press, Inc., Orlando, FL, 1985).
2. G. Agrawal, *Nonlinear Fiber Optics* (Academic Press, 1989).
3. J. Leuthold, C. Koos, and W. Freude, "Nonlinear silicon photonics," Nat. Photonics **4**, 535–544 (2010).
4. M. Soljačić, M. Ibanescu, S. G. Johnson, Y. Fink, and J. D. Joannopoulos, "Optimal bistable switching in nonlinear photonic crystals," Phys. Rev. E **66**, 055601 (2002).
5. I. V. Kabakova, T. Walsh, C. M. de Sterke, and B. J. Eggleton, "Performance of field-enhanced optical switching in fiber bragg gratings," J. Opt. Soc. Am. B **27**, 1343–1351 (2010).
6. B. E. A. Saleh, M. C. Teich, and B. E. Saleh, *Fundamentals of Photonics*, vol. 22 (Wiley Online Library, 1991).
7. L. L. Goddard, J. S. Kallman, and T. C. Bond, "Rapidly reconfigurable alloptical universal logic gates," Proc. SPIE **6368** 63680H (2006).
8. W. Chen and D. L. Mills, "Gap solitons and the nonlinear optical response of superlattices," Phys. Rev. Lett. **58**, 160–163 (1987).
9. C. M. de Sterke and J. E. Sipe, "Gap solitons," Prog. Optics **33**, 203–260 (1994).
10. B. J. Eggleton, C. M. de Sterke, A. B. Aceves, J. E. Sipe, T. A. Strasser, and R. E. Slusher, "Modulational instability and tunable multiple soliton generation in apodized fiber gratings," Opt. Comm. **149**, 267–271 (1998).
11. N. G. R. Broderick, "Bistable switching in nonlinear bragg gratings," Opt. Comm. **148**, 90–94 (1998).
12. F. Eilenberger, C. M. de Sterke, and B. J. Eggleton, "Soliton mediated optical quantization in the transmission of one-dimensional photonic crystals," Opt. Express **18**, 12708–12718 (2010).
13. A. Figotin and I. Vitebskiy, "Slow wave phenomena in photonic crystals," Laser Photon. Rev. **5**, 1863–8899 (2010).
14. P. Colman, C. Husko, S. Combrié, I. Sagnes, C. W. Wong, and A. De Rossi, "Temporal solitons and pulse compression in photonic crystal waveguides," Nat. Photonics **4**, 862–868 (2010).
15. A. Figotin and I. Vitebskiy, "Frozen light in photonic crystals with degenerate band edge," Phys. Rev. E **74**, 066613 (2006).
16. N. Gutman, L. C. Botten, A. A. Sukhorukov, and C. M. de Sterke, "Degenerate band edges in optical fiber with multiple grating: efficient coupling to slow light," Opt. Lett. **36**, 3257–3259 (2011).

#175307 - $15.00 USD Received 5 Sep 2012; revised 11 Oct 2012; accepted 11 Oct 2012; published 19 Nov 2012

17. N. Gutman, C. M. de Sterke, A. A. Sukhorukov, and L. C. Botten, "Slow and frozen light in optical waveguides with multiple gratings: Degenerate band edges and stationary inflection points," Phys. Rev. A **85**, 033804 (2012).
18. A. A. Sukhorukov, C. J. Handmer, C. M. de Sterke, and M. J. Steel, "Slow light with flat or offset band edges in few-mode fiber with two gratings," Opt. Express **15**, 17954 (2007).
19. A. A. Sukhorukov, A. V. Lavrinenko, D. N. Chigrin, D. E. Pelinovsky, and Y. S. Kivshar, "Slow-light dispersion in coupled periodic waveguides," J. Opt. Soc. Am. B **25**, C65–C74 (2008).
20. P. Blown, C. Fisher, F. Lawrence, N. Gutman, and C. M. de Sterke, "Semi-analytic method for slow light photonic crystal waveguide design," Phot. Nano. Fund. Appl. In Press (2012).

## 1. Introduction

All-optical switching is the phenomenon by which the reflection or transmission of an optical system changes very rapidly upon a small change of input intensity [1]. Since the fast nonlinear effects which are of interest here tend to be weak, leading to high switching intensities, all-optical switching experiments are invariably carried out in guided-wave geometries where the light is transversely confined, enhancing the field strength [2]. This field confinement is particularly strong in high-index semiconductor nanowires, since their cross section is of the order of the square of the wavelength inside the material [3]. Confinement in all three dimensions, such as in cavities (Fabry-Perot, photonic crystal cavities, ring resonators) further enhances the field strength. The enhancement increases with the cavity quality factor [4]. High field intensities inside a cavity enhance the response to input power change [5], however when using cavity resonances to enlarge the optical field, bistability occurs which results in switching hysteresis [6]. It has been argued by Goddard et. al. [7] that the bistable regions are undesirable for all-optical switching and all optical logic, since hysteresis loops in bistable devices can cause ambiguity and increase bit error rates.

Optical fields can also be enhanced using slow light , such as found near a photonic band edge. All-optical switching with slow light, particularly in one-dimensional gratings, has been studied for many years, both theoretically [8, 9] and experimentally [10]. The propagation of high-intensity light near a photonic band edge leads to a nonlinear shift of the band structure so that, at a fixed frequency, previously forbidden states become allowed states, or *vice versa*, leading to switching [11]. However, such switching is accompanied by bistable regions [12].

Near a regular photonic band edge (RBE) where the frequency $\omega$ and the wavenumber $k$ are related by $\Delta\omega \propto \Delta k^2$ [see Fig. 1(a), red], the group velocity is $v_g = \partial\omega/\partial k \propto \Delta k$, and the local field intensity for a given energy flux scales as $v_g^{-1}$. Despite the ubiquitous nature of slow light near a RBE, in practice no energy buildup occurs. Because of the impedance mismatch between the incoming light and the slow light, the energy coupling at RBE decreases proportionally to $v_g$, which prevents any field enhancement [13]. Different methods have been developed to overcome the poor coupling at moderately low group velocities around $c/40$, where $c$ is the speed of light in vacuum. These include apodization [10] and inverse tapers [14]. However these approaches are not scalable for smaller group velocities, since they rely on an intermediate structure with a length which increases proportionally to the slow-down factor.

Unlike the slow light at RBEs, near *degenerate band edges* (DBEs) for which $\Delta\omega \propto \Delta k^4$ [see Fig. 1(a), blue], light couples efficiently to low and even zero group velocity modes corresponding to the "Frozen Light" regime [15, 13]. We have previously shown that this favorable coupling is due to the presence of evanescent modes with complex wavenumbers [16, 17]. The complex dispersion relation of a DBE, showing frequency versus the real and imaginary parts of the wavenumber, is shown in Fig. 1(d). Close to a DBE, the dispersion of evanescent and slow propagating modes is found as $\Delta k_j = \sqrt[4]{\xi\Delta\omega}\exp(i\pi j/2)$ [17]. Here $\Delta k$ and $\Delta\omega$ are the wavenumber and frequency detuning from the DBE, respectively, $j = 0,2$ for the propagating mode and $j = 1,3$ for the evanescent modes, and $\xi$ is a real constant characteristic of the DBE dispersion (Media 2). In Fig. 1(d), the black curves represent the evanescent waves with

#175307 - $15.00 USD Received 5 Sep 2012; revised 11 Oct 2012; accepted 11 Oct 2012; published 19 Nov 2012

complex $k$, and blue — propagating modes with real $k$. The existence of evanescent modes highlights the difference between DBEs and RBEs: in RBEs [Fig. 1(c) (Media 1)] evanescent modes exist only inside the photonic band gap, whereas at DBEs propagating and evanescent modes coexist in the transmission band.

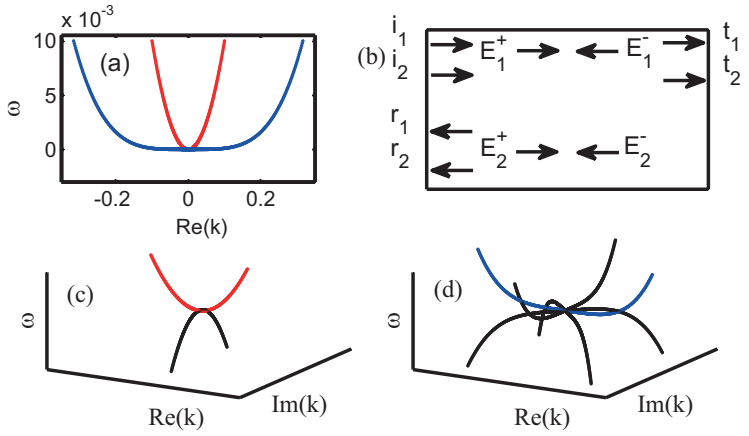


Fig. 1. (a) Dispersion of propagating modes at a RBE (red) and DBE (blue). (c-d) Complex band structure of (c) RBE (Media 1) and (d) DBE (Media 2). Blue and red curves correspond to the propagating modes with real wavenumbers as shown in (a), black curves represent evanescent modes with complex wavenumbers. (b) Two-mode waveguide where DBE can be realized.

In this work, we suggest and demonstrate through numerical modeling that the presence of the evanescent modes near a DBE can strongly enhance nonlinear effects and accordingly lower the threshold for all-optical switching. In Section 2 we formulate the coupled-mode theory used to analyze waveguides with a DBE. In Sec. 3 we analyze power-dependent transmission and reveal that bistability and hysteresis can be suppressed by choosing the excitation conditions. We present conclusions in Sec. 4.

## 2. Coupled mode description

Degenerate Band Edges can be created in a variety of periodic guided-wave structures [17], such as fiber Bragg gratings [18], nanowires [19] and photonic crystal waveguides [20]. The solutions for light propagation in such structures can be found using full 3D vectorial solvers such as finite difference time domain (FDTD) and transfer matrix methods, however these are computationally intensive and can be ill-suited for nonlinear problems. Perturbative approaches such as *coupled mode theory* (CMT) and the *nonlinear Schrödinger equation* (NLSE) are better suited as they are efficient and can provide a physical insight. Here we use CMT, which can account for both the propagating and evanescent modes.

In order to model a periodic waveguide with a DBE, we start with a longitudinally uniform waveguide with two types of modes: the fundamental and a higher-order mode with propagation constants $\tilde{K}_1$ and $\tilde{K}_2$, respectively, both at a given frequency $\tilde{\Omega}$. The total field is thus characterized by four amplitudes $E^{\pm}_{1,2}$, where the signs correspond to forward $(+)$ and backward $(-)$ propagation. We take the modulus of group velocity $v$ and the refractive index $n$ of these modes to be the same. In the presence of the periodic modulation ("grating"), the modes can be coupled and the amplitudes become envelopes $E^{\pm}_{1,2}(z,t)$ that vary in space and time. Two gratings are sufficient to realize a DBE: one grating, with coupling coefficient $\rho_1$ and period

#175307 - $15.00 USD Received 5 Sep 2012; revised 11 Oct 2012; accepted 11 Oct 2012; published 19 Nov 2012

$2\pi/(2\tilde{K}_1)$, couples Mode 1 to its counter-propagating counterpart. The other grating, with the coupling coefficient $\rho_2$ and period $2\pi/(\tilde{K}_1+\tilde{K}_2+\delta)$, couples Mode 1 to the counter propagating Mode 2 [17]. The grating coupling and Kerr nonlinear interactions between the modes can be described by the coupled-mode equations [18],

$$\begin{aligned} & i\frac{\partial E_1^{\pm}}{\partial t} \pm iv\frac{\partial E_1^{\pm}}{\partial z} + \rho_1 E_1^{\mp} + \rho_2 E_2^{\mp} \\ & \quad + [\Gamma_{11}(|E_1^{\pm}|^2 + 2|E_1^{\mp}|^2) + 2\Gamma_{12}(|E_2^{\pm}|^2 + |E_2^{\mp}|^2)]E_1^{\pm} + 2\Gamma_{12}E_2^{\pm}E_2^{\mp}E_1^{\mp *} = 0, \\ & i\frac{\partial E_2^{\pm}}{\partial t} \pm iv\frac{\partial E_2^{\pm}}{\partial z} \pm \delta E_2^{\pm} + \rho_2 E_1^{\mp} \\ & \quad + [\Gamma_{22}(|E_{22}^{\pm}|^2 + 2|E_2^{\mp}|^2) + 2\Gamma_{12}(|E_1^{\pm}|^2 + |E_1^{\mp}|^2)]E_2^{\pm} + 2\Gamma_{12}E_1^{\pm}E_1^{\mp}E_2^{\pm *} = 0, \end{aligned} \tag{1}$$

where the coefficients are $\rho_j = \tilde{\Omega}\Delta n_j/(2n^2)\int\int g_1 g_j dxdy$ and $\Gamma_{ij} = 3\chi^{(3)}/(2n^2\tilde{\Omega})\int\int g_i^2 g_j^2 dxdy$ respectively, $g_{i,j}(x,y)$ are the modal cross sections, $\Delta n_j$ are the amplitudes of the refractive index modulations in gratings, and $\chi^{(3)}$ is the 3rd order nonlinear susceptibility. The $\Gamma$'s can be expressed in terms of the nonlinear refractive index as $\Gamma = 4\pi n^{(2)}/(\lambda Z)$, where $Z$ is the vacuum impedance, $\lambda$ the optical wavelength, and $n^{(2)}$ is in the units of $\mathrm{W}/\mathrm{m}^2$.

At low intensities the nonlinear terms in Eqs. (1) can be ignored. We can then find the linear dispersion relation by substituting plane-wave solution of the form $E_{1,2}^{\pm}(z,t) = C_{1,2}^{\pm}e^{i(kz-\omega t)}$, where $\omega$ and $k$ are the frequency and wavenumber detuning from $\tilde{\Omega}$ and the associated wavenumbers $\tilde{K}_{1,2}$, respectively. We choose $\omega$ to be real and find the associated $k$ as eigenvalues which are either real, or come in complex conjugate pairs. We then adjust the linear parameters $\rho_{1,2}$ and $\delta$ so that the dispersion relation has a DBE at its upper band edge. We find that for most $\rho$'s it is sufficient to adjust only $\delta$ in order to eliminate the quadratic dependence of the band edge and turn it into a quartic DBE. In this paper we take these parameters to have the values $\delta = -1.7166$, $\rho_1 = 1$ and $\rho_2 = 0.5$, and we adjust the length scale such that $v = 1$. The eigenvectors, the *grating modes*, are superpositions of the uniform waveguide modes, and can be either propagating ($k$ real) or evanescent ($k$ complex). The complex dispersion of propagating and evanescent modes for these parameters is shown in Fig. 1(d).

## 3. Results

We now consider a DBE waveguide of a finite length of $\rho_1 L = 12$, in normalized units [9]. This normalized length corresponds approximately to 8 cm in a silica fiber grating and 20 $\mu$m in a perforated silicon nanowire, where the refractive index modulation depths are in order of $10^{-4}$ and 1, respectively. We note that the fundamental fiber mode has a nonlinearity which is much larger than that of the other modes, *i.e.*, $\Gamma_{11} \gg \Gamma_{12} \gg \Gamma_{22}$. Therefore, in our analysis below we only include $\Gamma_{11} \equiv \Gamma$, and put $\Gamma_{12} = \Gamma_{22} = 0$. We have ascertained that this does not qualitatively affect our results, which can therefore predict the general switching features in nanowire waveguides, for which $\Gamma_{11}$ also dominates as well.

We first consider the low-intensity limit and solve for CW light tuned to the band edge frequency $\omega_D$, incident from a uniform section of the waveguide. Since the waveguide has two different modes, the complex amplitudes $i_{1,2}$ of which can be independently adjusted, the input can be parameterized, by two real parameters $\alpha$ ($0 < \alpha < \pi/2$) and $\beta$ ($-\pi < \beta < \pi$), where $i_1 = \cos(\alpha)\exp(i\beta)$, and $i_2 = \sin(\alpha)$. Figure 2(a) shows the reflection from the structure versus $\alpha$ and $\beta$. In Fig. 2(b) we plot the field inside the waveguide at the two points marked A and B in Fig. 2(a), where, respectively, the reflection is lowest and highest.

For the band edge frequency at the condition B, almost all the light is reflected back and the field decays into the grating, similar to the behavior of a RBE. In contrast, at condition A we get frozen light: the reflection is only slightly less, but the energy builds up inside the waveguide.

#175307 - $15.00 USD Received 5 Sep 2012; revised 11 Oct 2012; accepted 11 Oct 2012; published 19 Nov 2012

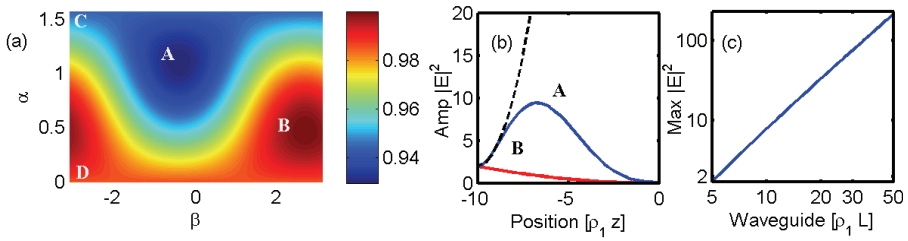


Fig. 2. (a) Reflection versus the input parameters ($\alpha$, $\beta$) at the DBE frequency for a waveguide of length $\rho_1 L = 12$. (b) Field intensity inside the waveguide for the condition of minimum (blue) and maximum (red) reflection, corresponding to points A and B in (a), respectively. Dashed black line shows asymptotic for the blue line at small $z$. (c) Field enhancement inside the waveguide versus waveguide length (loglog scale) at input state A, showing that the enhancement is $\propto L^2$.

The total field initially grows as $z^2$ before it decays, where $z$ is the distance from the interface. This quadratic dependence is shown with a black dashed line in Fig. 2(b). For an infinitely long frozen light waveguide, at the DBE frequency all the light is reflected back, but remarkably the field diverges as $z^2$. This was originally predicted by Figotin and Vitebskiy [13] for a different geometry, and we confirm that it occurs at a DBE in the framework of the model in Sec. 2. Indeed, Fig. 2(c) shows that at the condition A the maximum field is proportional to $(\rho_1 L)^2$. The reason for the divergence of the field is due to the degeneracy between the propagating and the evanescent grating modes at the DBE frequency. To satisfy the boundary condition, they must span the input profile, $V_i = [i_1, i_2]^T = \mathrm{span}(\mathrm{V_{pr}}, \mathrm{V_{ev}})$. An input profile which is orthogonal to $V_i$, which corresponds to condition A in Fig. 2(a), requires $V_{pr}$ and $V_{ev}$ to have large amplitudes. At the condition B, $V_i$ is parallel to $V_{er}$ and $V_{pr}$ and each has a small amplitude.

We now consider the high-intensity regime with positive nonlinearity. This has the effect of increasing the refractive index with intensity, thus shifting the band structure to lower frequencies, leading to an increase in transmission for frequencies near the top of the band edge. To find the nonlinear stationary solutions, we solve Eqs (1) by backward integration of a given output field, $E(0) = [\sqrt{S_t}(t_1, t_2), (0,0)]^T$, where $S_t$ is the total transmitted flux and $\sqrt{|t_1|^2 + |t_2|^2} = 1$. After integration, we find $\mathbf{E}(-L) = [\sqrt{S_i}(i_1, i_2), \sqrt{S_r}(r_1, r_2)]^T$, where $S_i$ and $S_r$ are the incident and reflected flux respectively and $\sqrt{|i_1, r_1|^2 + |i_1, r_2|^2} = 1$. Because in experiment the inputs ($i_1$ and $i_2$) are directly controlled, the output ($t_1$ and $t_2$) were searched numerically in order to match the inputs after integration. In Fig. 3(a) we show the total transmission versus the input flux ($S_i$) at the band edge frequency for the monomode cases: $\alpha = \beta = 0$ (blue) and $\alpha = \pi/2$, $\beta = 0$ (red), corresponding to the conditions C and D [Fig. 2(a)] respectively. We have determined the stability of stationary solutions with respect to small perturbations, and show the linearly stable branches with the continuous curves and unstable states with plus signs.

Figure 3(b) compares the transmission versus the input flux between DBE at the condition *A* and at a RBE with the same length, $\rho_1 L = 12$. We see that in both cases the transmission is a strongly nonlinear function of the input power, which can be used for optical switching. The key difference is that the transmission curve for a RBE is bistable, whereas for a DBE with the input condition *A* there is no bistability. Another key difference between a DBE and RBE is that while for a RBE the threshold slightly increases with length, for an DBE it decreases as $L^{-2}$ (Fig. 3(c)). This happens due to the strong field enhancement inside the waveguide with DBE at both low and high intensities, see Figs. 2(b) and 3(d) respectively. We also point out that unstable solutions [$(+)$'s in Figs. 3(a-b)] give rise to self-pulsations associated with gap-soliton excitations at much lower powers in DBE than in RBE.

#175307 - $15.00 USD Received 5 Sep 2012; revised 11 Oct 2012; accepted 11 Oct 2012; published 19 Nov 2012

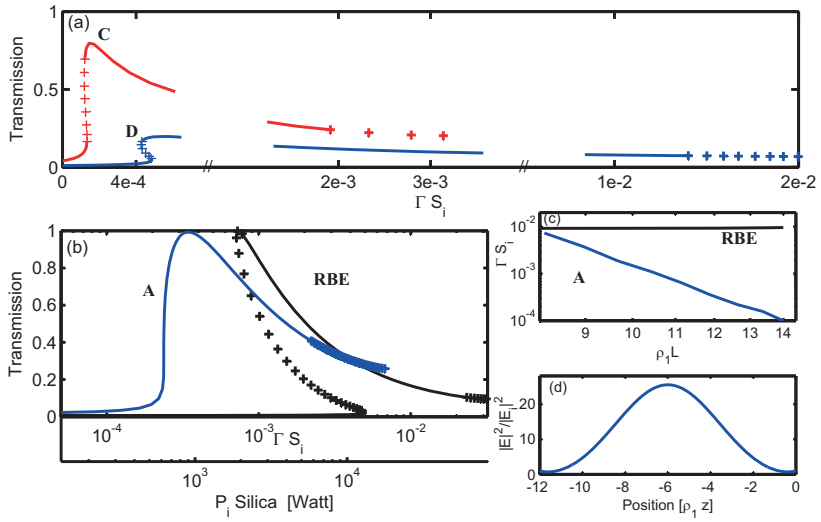


Fig. 3. (a-b) Transmission vs. the input flux at the band edge frequency: (a) the DBE with input amplitudes $i_1 = 1$ (red) and $i_2 = 1$ (blue), corresponding to points C and D in Fig. 2(a), respectively; (b) the DBE with input amplitudes corresponding to point A in Fig. 2(a) (blue) and a RBE (black). Solid lines indicate stable while and plus $(+)$ signs — unstable stationary solutions. (c) Threshold power for switching (100% transmission) versus the normalized waveguide length. (d) Field profile inside the waveguide at the nonlinear resonance.

Finally, we compare the switching threshold between the DBE and RBE in a fiber grating made of silica. For a RBE there is only a single mode and one grating, and for comparison with DBE we take the grating coefficient as $\rho = \rho_1 = 1$. In an additional scale the Fig. 3(b) we give the input flux rescaled using the effective cross section of 20 $\mu$m$^2$ and $n^{(2)} = 2.86 \times 10^{-20}$ W/m$^2$ for silica fiber. Note that the threshold exceeds 10 kW for an RBE, whereas for the same length fiber with a quartic DBE the threshold is 800 W.

## 4. Conclusions

We have predicted strong slow-light enhanced all-optical switching near the degenerate band edge of nonlinear waveguides. Such waveguides support frozen light at the band edge frequency and this facilitates strong field increase inside the waveguide. As a consequence, nonlinear effects are strongly enhanced at DBEs, which enables low-threshold all-optical switching. While in conventional cavity structures the field is enhanced due to multiple reflections in the cavity, here the enhancement is based on a different physical mechanism involving the interference of near-degenerate slowly propagating and evanescent modes. The threshold for the all-optical switching between the low and full transmission can be flexibly designed, as it scales inversely proportional to the squared length of the waveguide. Moreover, in the frozen light regime the bistability and hysteresis can be avoided. Our estimates indicate that such switching can be realized in silica fibers and nanowire waveguides.

## Acknowledgments

This work was supported by the Australian Research Council programs, including Discovery Project DP1093445 and Future Fellowship FT100100160.

#175307 - $15.00 USD Received 5 Sep 2012; revised 11 Oct 2012; accepted 11 Oct 2012; published 19 Nov 2012